Bioresource Technology 297 (2020) 122436

Contents lists available at ScienceDirect

Bioresource Technology

journal homepage: www.elsevier.com/locate/biortech

Case Study

Dissolved carbon monoxide concentration monitoring platform based on direct electrical connection of CO dehydrogenase with electrically accessible surface structure

Stacy Simai Reginald[a,1], Hyeryeong Lee[a,1], Yoo Seok Lee[a], Muhammad Yasin[a,b], In Seop Chang[a,*]

[a] School of Earth Sciences and Environmental Engineering, Gwangju Institute of Science and Technology (GIST), 123 Cheomdan-gwagiro, Buk-gu, Gwangju 61005, Republic of Korea

[b] Bioenergy & Environmental Sustainable Membrane Technology (BEST) Research Group, Department of Chemical Engineering, COMSATS University Islamabad (CUI), Lahore Campus, Pakistan

GRAPHICAL ABSTRACT

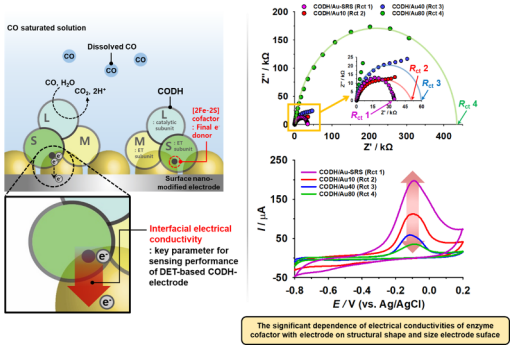

ARTICLE INFO

Keywords:
Syngas fermentation
CO biosensor
Carbon monoxide dehydrogenase (CODH)
Direct electron transfer (DET)
Surface relief structure (SRS)

ABSTRACT

CO dehydrogenase (CODH) employed in a dissolved CO biosensor development study harbors a solvent-exposed cofactor capable of DET to electrode. Here, CODH was immobilized on arrays of AuNPs of various dimensions to determine the effect of the size and shape of the electrode surface on the direct electrical connection between CODH and electrode surface. The results showed the degree of proximity between the CODH cofactor and electrode surface, which varied with AuNP size and caused significant changes to the electrical connection at the interface as well as to the substrate accessibility. Consequently, a high-density nanoscale SRS was fabricated on electrode to further facilitate direct electrical connection as well as to enable distribution of CODH into monolayer or near-monolayer for lowering the barrier of CO diffusion toward enzyme. The findings show the feasibility of controlling the direct electrical connection between CODH and the electrode as well as controlling the substrate accessibility.

* Corresponding author.
E-mail address: ischang@gist.ac.kr (I.S. Chang).
[1] These authors contributed equally to this work

https://doi.org/10.1016/j.biortech.2019.122436
Received 30 September 2019; Received in revised form 9 November 2019; Accepted 12 November 2019
Available online 15 November 2019
0960-8524/

1. Introduction

Microbial conversion of syngas to biochemical and biofuels has emerged as a promising technology for the environmentally friendly use of coal and biomass (Yasin et al., 2015). Carbon monoxide (CO), a major component of syngas and industrial waste gases from the steel industry, is an important feedstock for C1 biorefinery. However, commercial syngas fermentation is limited due to several constraints including the low solubility and mass transfer of CO in fermentation medium (mass transfer limitation), as well as the toxicity of high concentrations of CO to microbes (kinetic limitation) (Yasin et al., 2015). The development of an ideal bioprocess for bioconversion of CO depends on designing an optimal bioreactor system, which would ideally operate under no substrate limitation and inhibitory conditions. This pursuit can be accomplished by maintaining the concentration of dissolved CO (C_{co}) in an optimal range during continuous bioreactor operation (Jeong et al., 2016). Notably, the C_{co} in the reactor depends on the overall volumetric mass transfer coefficient (k_La) and pressure inside the reactor (Jang et al., 2017). However, a fixed k_La can only support continuous microbial growth up to certain cell concentrations during long-term operation (Jeong et al., 2016). Thus, the k_La required for CO fermentation on a large scale would not stay the same during the entire operation, but instead would depend on the available microbial population. Since the C_{co} in the reactor is a prerequisite for maintaining the optimal C_{co} range and finding the operating k_La of the reactor, determining the actual C_{co} levels is essential for predicting the precise microbial activity. This determination can only be done by continuously monitoring the C_{co} levels in the reactor.

All syngas fermentation studies reported to date employ a gas-chromatography-based method applying Henry's law and the CO partial pressure in the headspace to indirectly estimate C_{co} in the aqueous phase. Another common method here involves a myoglobin-protein bioassay. These methods are not only tedious but also time consuming and limited to off-line measurement (Munasinghe and Khanal, 2014). Thus, developing an integrated system providing quantitative real-time analytical tools in the syngas fermentation reactor to allow monitoring and controlling of the process would be of a great value.

Enzyme-based biosensors are promising candidates for use in such systems due to their specificity and high sensitivity as well as regeneration ability (Ispas et al., 2012). The enzyme-based biosensor developed in the current work makes use of the native ability of the key enzyme in CO oxidation, namely carbon monoxide dehydrogenase (CODH), which can be found in some anaerobic bacteria that utilize the Wood-Ljungdahl pathway and in some aerobic carboxydotrophic bacteria (Ragsdale, 2008). CODH catalyzes the oxidation of CO to CO_2, which generates two electrons per molecule converted; this generation of electrons can be quantified as an electric current, which is used to quantify C_{co} in solution. The application of aerobic CODH is more practical than is that of its anaerobic CODH counterpart due to the extreme sensitivity of the latter to oxygen. The aerobic CODH from *Hydrogenophaga pseudoflava* has been intensely studied in the past years. Its crystal structure and functions have been determined and are essential for a deep understanding of the enzyme, which is expected to be used in the development of the enzyme-based biosensor. Thus, in the current study, the aerobic CODH from *H. pseudoflava* was used as the source of enzyme for the fabrication of the enzyme-electrode used for oxidizing CO in aqueous solutions.

Overall, in enzyme-based bioelectronics, the mechanism of the electronic coupling of redox enzymes to electrodes for the development of analytical devices such as biosensors depends on the presence of an electron transfer (ET) subunit, and the needs for mediator which determine the ET mechanism to be direct electron transfer (DET) or mediated electron transfer (MET) (Freire et al., 2003).

For DET at the enzyme-electrode interface to take place, several conditions must be met: 1) the enzyme cofactor or the last electron donor should be close to the electrode surface (Marcus and Sutin, 1985; Milton and Minteer, 2017; Lee et al., 2018a); 2) the cofactor site serving as the final electron donor should not be hindered by external agents such as adjacent enzymes (Kamin and Wilson, 1980; Houseman and Mrksich, 1999; Love et al., 2005); and 3) the substrate for the enzyme catalytic reaction should be able to access the enzyme with minimal hindrance to its diffusion. For sensing of dissolved CO and determination of its concentration, the accessibility of the substrate (CO) is especially critical considering the low solubility of gaseous CO in the aqueous phase (Maly et al., 2005; Zebda et al., 2011).

Especially with the low-CO solubility, low C_{co} and related other conditions of syngas fermentation systems, agglomeration of enzyme molecules on the electrode, which is generally caused by the intrinsic nature of enzymes producing hydrophobic interactions between the enzyme molecules, could exacerbate the limits on the mass transfer of CO substrate toward the enzyme cofactor. At the same time, the formation of densely multi-stacked enzymes impedes the access of electrons from the enzyme cofactor in the upper layer to the electrode and limits the access of substrate to the enzyme cofactor in the underlying enzyme layer, which is in direct contact with the electrode, and hence diminishes the ability of the biosensor to detect dissolved CO (Nylander et al., 1996; Mutlu et al., 1998). Thus, fabricating a monolayer or near-monolayer of enzymes on the electrode should be pursued to facilitate close contact of the enzyme cofactor (final electron donor) with the electrode and promote better mass transfer of the substrate, thereby increasing the relative amount of bioactive enzyme as well as enhancing the ET kinetics at the enzyme-electrode interface. To achieve such a fabrication, fine-tuning of the structural shape and size of the electrode could be a promising approach, and could specifically facilitate a distribution of enzymes on the electrode where a greater proportion of the enzymes on the electrode have close contact with electrode surface and also facilitate access of the substrate to the immobilized enzymes on the electrode surface (Ding et al., 2010; Goran et al., 2013; Do et al., 2015).

In a DET-capable enzyme possessing an electron transfer subunit, the surroundings of a cofactor embedded in the enzyme matrix as well as the interface of the enzyme cofactor and electrode would be in a nanoscale environment. Thus, subtle changes to the structure of the electrode where the enzyme is directly bound could particularly influence the degree of the proximity of the cofactor to the electrode together with the distribution of enzymes bound on the electrode, which importantly determines the electrical conductivity of the enzyme cofactor with the electrode.

In this vein, the relationship between surface structure and the electrical connection between the enzyme active center and the electrode surface was initially investigated by immobilizing CODH on arrays of Au nanoparticles (AuNPs) with each array having a different particle dimension. It is hypothesized that the degree of proximity between the enzyme cofactor and electrode would sensitively depend on the electrode surface structure to which the enzymes are anchored, and hence significantly affect the electrical conductivity of the enzyme cofactor with the electrode surface. It was assumed that the AuNPs with different sizes would result in different curvatures. Specifically, AuNPs with greater diameters would have lower curvatures. The resulting structural difference was assumed to result in different nano-environments at the enzyme-electrode interface, with the high curvature of an electrode binding surface potentially suppressing proteinous interactions with surrounding enzymes, thus alleviating enzyme agglomeration (Zhang et al., 2013). Controlling enzymatic agglomeration on the electrode led to substantial improvements in the mass transfer of substrate as well as ET kinetics according to electrochemical measurements.

The results of the experiments with AuNPs of various dimensions suggested that it is necessary to be able to control the nanoscale surface structure of the electrode surface in order to achieve the best possible direct electrical connection of the enzyme active site to the electrode, but that such control is only relevant to enzymes bearing electron

transfer subunits. Besides, modification of the nanoscale surface structure may help reduce enzyme agglomeration, which could affect the access of substrate to the enzyme redox site and electrical contact of the active site with the electrode. A surface relief structure (SRS) in this manuscript refers to the structure with high-respect ratio with fine period and tall height; the formation of such structures could render grassy surfaces with high roughness and a high density of features (Song et al., 2013). As the electrode for CODH, even though the structural feature of high surface area is excluded, the SRS has structural merits: 1) every surface of the SRS would face the bulk electrolyte, without any confined spaces, and hence no mass transfer limitation would be caused by a structural feature of the electrode; and 2) the high roughness of the surface would enable more enzymes to be distributed on the electrode without agglomerating and hence increase the bioactive species. Varničić et al. (2014) showed that a high roughness of a surface onto which enzymes are distributed would increase utilization of the enzyme on the electrode. Therefore, formation of an SRS is expected to promote the catalysis of CO oxidation by enzymes on the electrode and therefore enhance the electrochemical signal from the electron exchange between the enzyme and electrode, *via* reducing the enzymatic agglomeration and alleviating limits on the mass transfer of the CO substrate.

In the current study, in order to develop an enzyme biosensor for determining the concentration of dissolved CO, several procedures were performed: 1) oxygen-tolerant CODH from *H. pseudoflava* capable of DET was used; 2) immobilization of CODH on various gold nanoparticles having different diameters to assess the effect of surface structure on the enzyme morphology and ET thermodynamic and kinetic efficiency; 3) fabricated SRS electrode as a practical support for immobilized CODH and conducted electrochemical evaluation of this sensing platform; and 4) compared nano- and micro-structured electrodes, addressing the importance of nanofabrication of the electrode for efficient bioelectrocatalysis of enzymes on electrodes.

2. Materials and methods

2.1. Preparation of CODH from H. Pseudoflava

H. pseudoflava DSM 1034 from the Leibniz-Institute DSMZ - Deutsche Sammlung von Mikroorganismen und Zellkulturen GmbH (German Collection of Microorganisms and Cell Cultures) was cultivated in a mineral medium with CO as the sole energy and carbon source as described previously (Meyer and Schlegel, 1983).

Crude CODH was obtained using a previously described procedure, with modifications (Meyer et al., 2000). Cells were harvested at the late exponential phase by subjecting them to centrifugation at 5000 × g for 30 min at 4 °C. The cell pellets obtained were then washed with HEPES buffer (pH 7.2). The washed cells were suspended in 50 mM HEPES buffer containing 1 mM ethylenediaminetetraacetic acid, 5 mg lysozyme and 5 mg DNase *I*. Next, the resuspended cells were disrupted by subjecting them to sonication at 4 °C for 30 s. The sonication product was centrifuged at 17,000 rpm for 1 h at 4 °C and the resulting supernatant was used as an enzyme source.

Protein concentrations were estimated using the Bradford assay (Bradford, 1976). CODH activity was assayed spectrophotometrically (TS Science) at a wavelength of 615 nm by measuring the CO-dependent reduction of methylene blue (MB) (ε_{615} = 37.11 mM^{-1} cm^{-1}) in 50 mM phosphate buffer (PB) (pH 7.2) at 30 °C as described previously (Meyer et al., 2000). One unit of CODH activity indicates 1 μmol of CO oxidized per minute. The specific CODH activity obtained was 0.974 mU mg^{-1} protein.

2.2. Fabrication of nano- and micro-structured electrodes

2.2.1. Au nanoparticles array

AuNP-modified electrodes, AuNP arrays, the Au thin film were deposited on silicon (Si) substrates using an e-beam evaporator and annealed for 1 min using a rapid thermal annealing system (Ye et al., 2016). The thickness of the deposited Au film and annealing temperature were adjusted to make AuNPs with different diameters. The fabrication conditions including thickness of the deposited Au film and annealing temperature for each AuNP array are summarized in the supplementary information, together with mean dimension of AuNPs on each structure. Also, visualization of the fabricated AuNP arrays was conducted with a scanning electron microscope (SEM, S-4700, Hitachi, Japan). The mean diameter of the AuNPs was determined from the SEM images using a freeware image processing program (Image J 1.42q, NIH).

2.2.2. Au-subwavelength relief structure

The nanoscale SRS of a glass substrate was prepared by carrying out plasma etching in an RIE system with a mixture of CF_4 (40 sccm) and O_2 (10 sccm) gases. First, a borosilicate glass substrate, which is commonly used as an optical component in many fields, was cleaned with acetone, isopropyl alcohol, and deionized (DI) water and loaded into the chamber. Afterward, simultaneous process of self-masking and reactive etching of the unmasked area for grassy surface formation was done in one step. The pressure applied during this process was 50 mTorr and the RF power was 50 W. Finally, a 100-nm-thick Au film was deposited and post baked on a hot plate at 350 °C for 1 min to form the Au electrode with a nanoscale Au-SRS. Then, the topography of the prepared Au-SRS was analyzed using the scanning electron microscope (SEM, S-4700).

2.2.3. Au-coated carbon felt

A micro-structured gold matrix was prepared by depositing a gold film on a carbon felt. The carbon felt (C100 AvCarb) was purchased from Fuel Cell Earth (Woburn, MA). Then, the Au film was deposited on the carbon felt using an e-beam evaporator, to fabricate the Au-coated carbon felt (Au-felt).

2.3. Preparation of the CODH-electrode

To immobilize CODH on the electrode surface, the various types of prepared working electrodes including the plane Au electrode, AuNP arrays, Au-SRS, and Au-felt were each immersed in 3 mL of PB (50 mM, pH 7.2) containing CODH enzyme (100–400 μl), and each of these mixtures was stirred for 2 h.

2.4. Electrochemical measurements

All of the electrochemical experiments including cyclic voltammetry (CV), amperometry and electric impedance spectroscopy (EIS) were performed in a gas-tight reactor using a potentiostat (Metrohm AutoLab, Utrecht, Netherlands) in the PB (50 mM, pH 7.2) at 30 °C. A platinum wire and Ag/AgCl electrode were used as auxiliary and reference electrodes, respectively. The CV was performed at the potential range of the working electrode, i.e., from −800 to + 200 mV, at a scan rate of 50 mVs^{-1} unless otherwise stated. Then, EIS was performed under potentiostatic control in the frequency range 0.01 to 1.0 × 10^5 Hz.

3. Results and discussion

3.1. Use of an aerobic CODH electrode capable of direct electron transfer to monitor dissolved CO

The aerobic CODH from *H. pseudoflava*, which is known for its tolerance to oxygen and is capable of DET as we showed previously (Reginald et al., 2019), was immobilized on an Au electrode in a constructed gas-tight reactor. Aerobic CODH is a dimer of a heterotrimer, with three different subunits denoted as L, M and S. Subunit L contains

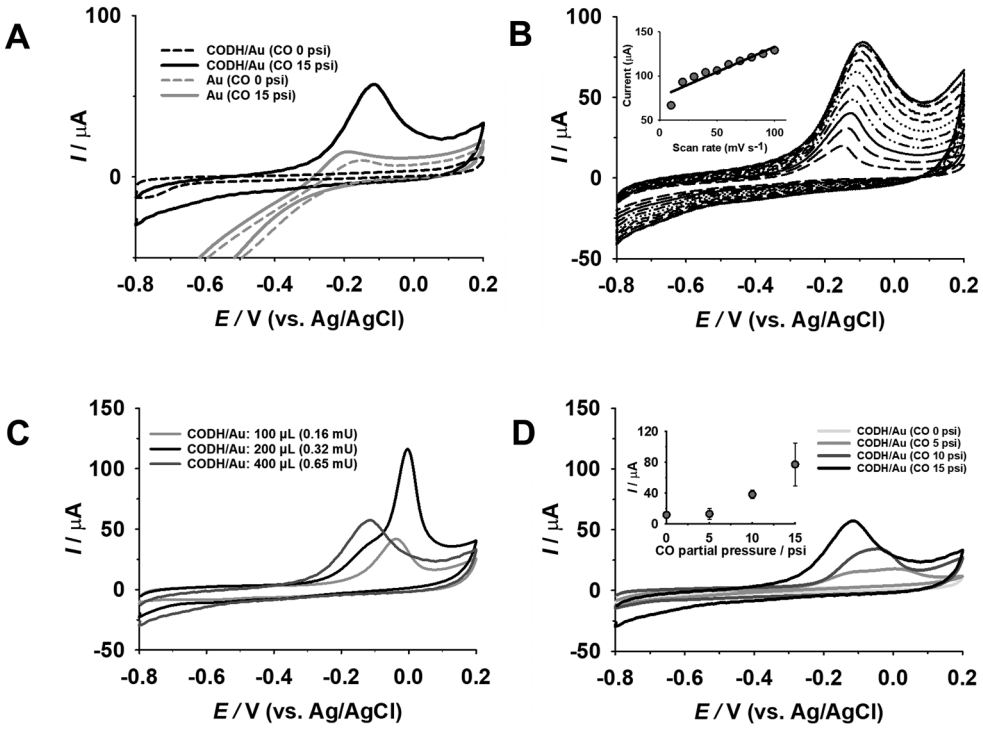

Fig. 1. (A) CV of bare Au, crude CODH immobilized Au in the presence and absence of 1 atm of CO. (B) CV recorded at various scan rates. (Inset) Plot of anodic current peak, I_{max} against scan rate. (C) CV recorded at various immobilized enzyme amount. (D) CV recorded under various CO partial pressure. (Inset) Peak current, I_{max} against CO partial pressure.

molybdenum-copper (Mo-Cu) where the CO oxidation takes place. Subunit M and subunit S, which are involved in providing the ET pathway, harbor flavin adenine dinucleotide (FAD) cofactor and two iron-sulfur [2Fe-2S] clusters, respectively (Dobbek et al., 1999, 2002).

The DET capacities of CODH on a plane Au electrode (CODH/Au) were examined using CV in the range −800 to + 200 mV (*vs.* Ag/AgCl) in PB (50 mM, pH 7.2) at 30 °C (Fig. 1A). Fig. 1A shows the CVs of bare and enzyme-immobilized plane Au electrodes in the presence and absence of CO. In the absence of CO, neither the bare Au electrode nor the CODH/Au showed a redox peak. In the presence of CO, CODH/Au showed a redox event at −255 mV (*vs.* Ag/AgCl). The significant increase in the oxidative current was a response to enzyme-catalyzed oxidation of CO.

Also, the dependence of the intensity of oxidative DET peaks on the scan rate (10–100 mVs^{-1}) was monitored. It was revealed that DET of CODH/Au proceeded as a surface-controlled process rather than a diffusion-controlled process since the increase of oxidative peak current was quite linearly related to the increase of scan rate (Fig. 1B).

The relationship between the catalytic CO oxidation current and the amount of biocatalyst or concentration of substrate was evaluated. To assess the effect of the amount of enzyme on the current response, various units of CODH, specifically 0.16 mU, 0.32 mU, and 0.65 mU, were immobilized on different electrode surfaces, respectively, followed by taking CV measurements at potentials from −800 to + 200 mV (*vs.* Ag/AgCl) in PB saturated with CO in which the dissolved concentration of CO was 0.964 mM, calculated from its saturated solubility. As shown in Fig. 1C, the electrocatalytic current was found to be correlated with the amount of immobilized CODH (measured in enzyme units), which suggested a profound effect of the amount of enzyme on the redox reaction level. The enzyme-electrode response towards various values of C_{co} was evaluated by performing CV experiments at various CO partial pressures (0–15 psi). According to Henry's law, the concentration of solute gas in a solution is directly proportional to the partial pressure of that gas above the solution. Thus, increasing the CO partial pressure increases the C_{co}. The enzyme-electrode response towards various CO partial pressures did not show strong correlation but enough to indicate that there was an increase in the current signal as the CO partial pressure was increased over specific potential ranges, showing a relative standard deviation of 14–55% (Fig. 1D).

The reproducibility of the direct electric communication between the enzyme and electrode in the presence of CO was also investigated. The anodic peak current during the application of five consecutive potential scans showed retention of almost 80% of the current, further confirming that the oxidation peak was indeed generated from the oxidation of CO catalyzed by enzyme immobilized on the electrode. To make up for demonstrating the catalytic turnover of dissolved CO by CODH fraction, steady-state amperometric responses to the successive injections of CO saturated solution performed additionally show current increases after each CO saturated solution spike.

However, even though detection of dissolved CO without the use of a mediator was successful, an overpotential and a significant slowing of the ET kinetics between the enzyme and electrode, which is the most significant issue for DET-based bioelectronic systems, did occur. In the CV tests, the ET mechanism was determined during a potential window scanning with a starting potential of −255 mV; the results provided evidence for an overpotential of DET between the Fe center [2Fe-2S] and the electrode, which displayed a formal potential ($E^{\circ\prime}$) of −593 mV (*vs.* Ag/AgCl) at pH 7.0. Importantly, while the intrinsic nature of CODH, in which one of the [2Fe-2S] clusters is generally exposed to solvent, would allow for DET between the enzyme and electrode, limitations on this DET could nevertheless occur; such limitations would be mainly due to random orientations of enzyme and too great of a distance between the cofactor and electrode for DET to occur due to the position of the enzyme cofactor in a narrow and deep cleft of the enzyme causing the enzyme active site to have few chances to be in electrical contact with the electrode. The hampered DET can be explained using Eq. (1).

$$R_{ct} = \rho L/A \quad (1)$$

In this equation, ρ is the resistivity of the material (in units of Ω m), L is the distance between the electron donor and acceptor (m), and A is the cross-sectional area of the electric current (m^2). In the case of an enzyme-electrode, L and A correspond to the ET distance and electrical contact area between enzyme cofactor and electrode surface, respectively. A location of a catalytic site deep inside the protein structure

could easily result in an increased ET distance, and hence an increased R_{ct}. The enzyme would have to adopt a specific orientation to result in the shortest possible distance between the redox cofactor and the electrode and hence the shortest possible ET distance. In addition, during immobilization of too many enzymes on the electrode, the electrical contact area could be limited due to obstruction of the enzyme cofactor by the non-conductive exteriors of surrounding enzymes, and hence result in an increased R_{ct}.

3.2. DET capacities of CODH-electrodes with different surface structures. The different structures reflected the use of different particle dimensions for the different arrays of AuNPs

The direct electrocatalytic activity of the CODH-electrode could be highly affected by the degree of proximity and electronic coupling between the final electron donor of the CODH enzyme and the electrode surface. The aerobic CODH complex, as mentioned above, consists of a dimer of heterotrimers, with two separate catalytic sites. Each monomer has one catalytic site at subunit L, FAD in subunit M, and two [2Fe-2S] cofactors – one embedded within the S subunit of the enzyme, and the other exposed externally (Dobbek et al., 2002). When the enzyme is directly bound to an electrode, the degree of proximity and electrical connection of the cofactor with the electrode surface would be expected to be highly dependent on the size and shape as well as material type of the electrode. The electrical connection of the enzyme cofactor to the electrode could be readily tailored by adjusting, on the nanometer level, the surface structure of the solid support. Considering the nanoscale nature of the surroundings of the cofactor embedded in the enzyme matrix as well as of the interface of the enzyme cofactor and electrode, a subtle change in the structure of the electrode where the enzyme is directly bound could significantly influence the extent of enzyme binding in addition to the degree of cofactor-electrode proximity.

In order to probe the characteristics of the electrode surface for enzyme electrocatalysis, DET-based monitoring of dissolved CO was tested by carrying out a procedure involving immobilizing CODH on various arrays of AuNPs with a different particle size, i.e., 10, 40, and 80 nm, for each different array. This approach was based on the idea that AuNPs with different dimensions would yield different levels of access to cofactors buried deep within the interior of the enzyme, and hence different conduction properties of the enzymatic cofactor with the surface of each AuNP array.

To probe the effects of the different AuNP arrays on the electrical access to the enzyme cofactor, CODH was immobilized on highly tuned AuNP electrodes denoted as Au10, Au40, Au80 (with the number next to 'Au' indicating diameters in nanometers of the AuNPs on the AuNP array) and electrochemical tests were performed. Immobilization of the enzyme on these different AuNP arrays (CODH/Au10, CODH/Au40, CODH/Au80) resulted in different enzyme-electrode interface conditions for DET. The DET capacities were examined using cyclic voltammetry (Fig. 2A). Following the addition of CO, each of the CODH-electrodes reacted with remarkable redox events. The catalytic current starting potential of CODH/Au10 was estimated to be about −320 mV, i.e., negatively shifted by 70 mV compared with the onset potential of CODH/Au. And a significant decrease in the overpotential for the electrocatalytic activity was observed for CODH/Au10 compared to that for CODH/Au. However, the onset potential of CODH on the AuNP array shifted positively as the AuNP diameter was increased, with CODH/Au80 displaying an onset potential of −240 mV, similar to that of CODH/Au. Moreover, CV peak current dramatically increased as the average diameter of the AuNPs on the electrode was decreased.

Next, the apparent Michaelis-Menten constant, K_M^{app}, was calculated for each enzyme electrode to investigate the influence of the cofactor-electrode electronic interaction (which was shown to depend on the electrode surface structure) on the enzyme catalytic activity toward CO oxidation. CV peak currents were measured for the various CODH-electrodes exposed to various CO partial pressures, from 0 to 15 psi (Fig. 2B). Using the linear part of the transient curves and Lineweaver-Burk transformation, the electrochemical K_M^{app} values were calculated to be 0.871, 1.51, 1.89, 1.85 mM for CODH on the Au10, Au40, Au80, and plane Au electrodes, respectively. The increase of K_M^{app} with increasing AuNP size implied that the enzyme catalytic activity became less favorable, possibly due to higher resistance to CO diffusion through the enzyme layer making it less likely for CO to reach the underlying enzymes near the electrode surface. As a result, and due to the inverse relationship between AuNP size and surface curvature, the enzymes may be concluded to have become well distributed as monolayers or near-monolayers when immobilized on electrode surfaces with higher curvatures. And thus, suppression of multi-stacking of enzyme layers, with the suppression due to immobilization of CODH on the electrode surface, could yield better CO affinity, suggesting facilitated mass transfer of the substrate to the enzyme catalytic site, and consequently a higher proportion of the surface of the enzyme electrode being conductive. In addition, the I_{max} obtained from the Lineweaver–Burk transformation (Fig. 2B) was 2.24-fold higher for CODH/Au10 than for CODH/Au (188.7 μA *vs.* 84.03 μA), suggesting that CODH molecules on Au10 were well distributed with increased electrical binding of the enzyme cofactor to the AuNPs as well as higher access of the substrate to the active sites.

EIS was employed to assess the electrical interaction between the AuNPs and enzyme cofactor for the various arrays of AuNPs, with each array displaying a different AuNP size (Fig. 2C). The R_{ct} values at the interface of the CODH cofactor and each of the Au10, Au40, Au80, and plane Au electrode surfaces were determined using EIS in order to analyze the DET conditions at the enzyme-electrode interfaces. Here, the R_{ct} was found to decrease as the AuNP units became finer, showing specifically values of 32.75, 58.85, 429.2, and 286.3 kΩ for CODH on Au10, Au40, Au80, and plane Au electrodes, respectively. The decrease of the interfacial R_{ct} of the enzyme-electrode with decreasing AuNP size could be rationalized as having been due to increased access of the enzymatic cofactor to the electrode surface. Smaller AuNPs would have been expected to more easily penetrate the deep cleft of the enzyme where the cofactor is located. In general, interfacial ET of an enzyme-electrode would be sluggish for the case of an ineffective electronic conductivity between the enzyme and electrode.

The results appeared to be in good agreement with the hypothesis that the electrical conductivity between the electrode surface and cofactor embedded in the ET subunit of the enzyme is highly dependent on the size and shape as well as material type of the electrode to which the enzyme is directly bound. In detail, the degree of proximity between the electrode surface and enzyme cofactor embedded in the enzyme matrix as well as enzyme distribution on the electrode was indicated to differ for different surface structures of AuNP arrays resulting from the different AuNP sizes. Consequently, the ET kinetics at the CODH-electrode interface as well as the enzyme activity of the immobilized CODH were found to differ significantly for the different types of AuNP arrays, i.e., those having different AuNP sizes (Fig. 2D).

3.3. Nanostructured and microstructured electrodes for CODH immobilization and DET kinetics for each electrode

To achieve high volumetric loading rates of enzymes on electrodes, various conductive electrode materials with high surface areas, such as carbon nanotubes, nanomeshes, and porous materials, have been introduced as solid supports for enzyme immobilization (Barsan et al., 2015; Chen et al., 2015; Lee et al., 2016). Despite the common expectation that these electrode materials with high surface areas would display high enzyme loading rates and thus higher catalytic activities, several other factors related to the electrocatalytic activities of enzymes on electrodes should be considered first for the purpose of optimizing the sensing performance of the CODH-electrode. Namely, enhancing the ability of each enzyme on the electrode to transfer electrons is essential

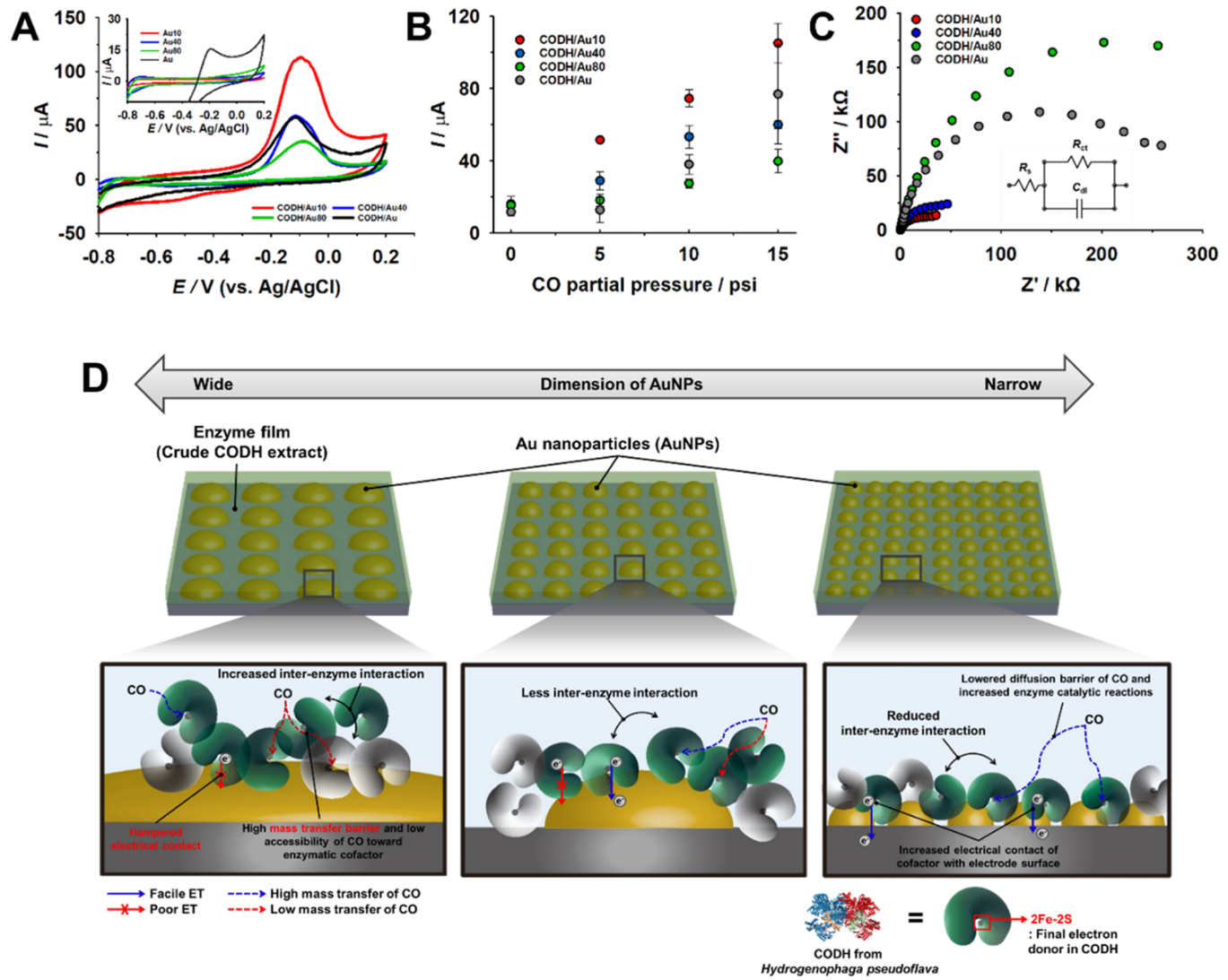

Fig. 2. (A) CV of bare Au, AuNP (Au10, Au40, and Au80) with and without crude CODH immobilized in the absence and presence of 1 atm of CO, respectively. (B) CV of crude CODH immobilized electrodes under various CO partial pressure. (C) Nyquist plots of crude CODH immobilized on Au10, Au40, Au80, and plane Au electrode. (D) Schematics for crude CODH immobilized on the AuNPs array with different diameters.

for increasing the proportion of electroactive enzymes on the electrode as well as the conductance of the enzyme cofactors with the electrode. Features that would improve the electrical conductivity of an enzyme cofactor with an electrode include 1) enzyme immobilization surrounding conditions favorable for the enzyme to retain its intrinsic catalytic activity on the electrode and 2) a close proximity of the enzyme cofactor to the electrode.

In the investigations of the effect of surface topography on the direct electrical connection of the enzyme active site to the electrode, which was performed with CODH on various AuNP arrays with each array displaying different AuNP sizes, smaller AuNPs (~10 nm) showed significantly different DET capacities, i.e., different levels of accessibility to the metallocofactor embedded within the enzyme matrix, than did the larger AuNPs. In addition, these results implied that a solid support with a nanolevel-controlled surface structure that is capable of providing electrical penetration into the enzyme cofactor would be preferred for achieving a higher conductivity of enzymes with electrodes, rather than a high-surface-area electrode with a microlevel- or macrolevel-controlled surface structure. Here, it could also be emphasized that a surface structure enabling close access of the enzyme cofactor to the electrode would be ideal for achieving a high conductivity of the enzyme cofactor with the electrode.

Considering the high loading of the enzymes on the electrode as well as electronic communication of each enzyme with the electrode, an Au-SRS was fabricated *via* a self-masked dry etching process. The SRS was a densely packed structure with no confined spaces; such a structure could help enhance electrical access of the enzyme cofactor with the electrode as well as facilitate distribution of enzyme molecules on the electrode, which may facilitate mass transfer of CO toward the enzyme redox site (Fig. 3 A). Also, Au-felt was fabricated as a microstructured Au electrode candidate and was compared with Au-SRS to address the importance of the scale of the control of the electrode surface. Then, the DET capacities of enzyme-electrodes were examined using CV and EIS (Fig. 3B–D).

Following the addition of CO, the CODH/Au-SRS showed a much stronger redox event than did the other conditions tested, and showed a response to enzyme-catalyzed CO oxidation starting at about −340 mV (*vs.* Ag/AgCl), which was negatively shifted by 90 mV compared to that of CODH/Au. The onset potential of CODH on Au-felt (CODH/Au-felt) was shown to be similar to that of CODH/Au, although CODH was immobilized onto the complex electrode structure, which is generally assumed to yield better ET efficiency at the enzyme-electrode interface.

The CV peak current was observed to be markedly increased at both CODH/Au-SRS and CODH/Au-felt, and their overall currents were quite

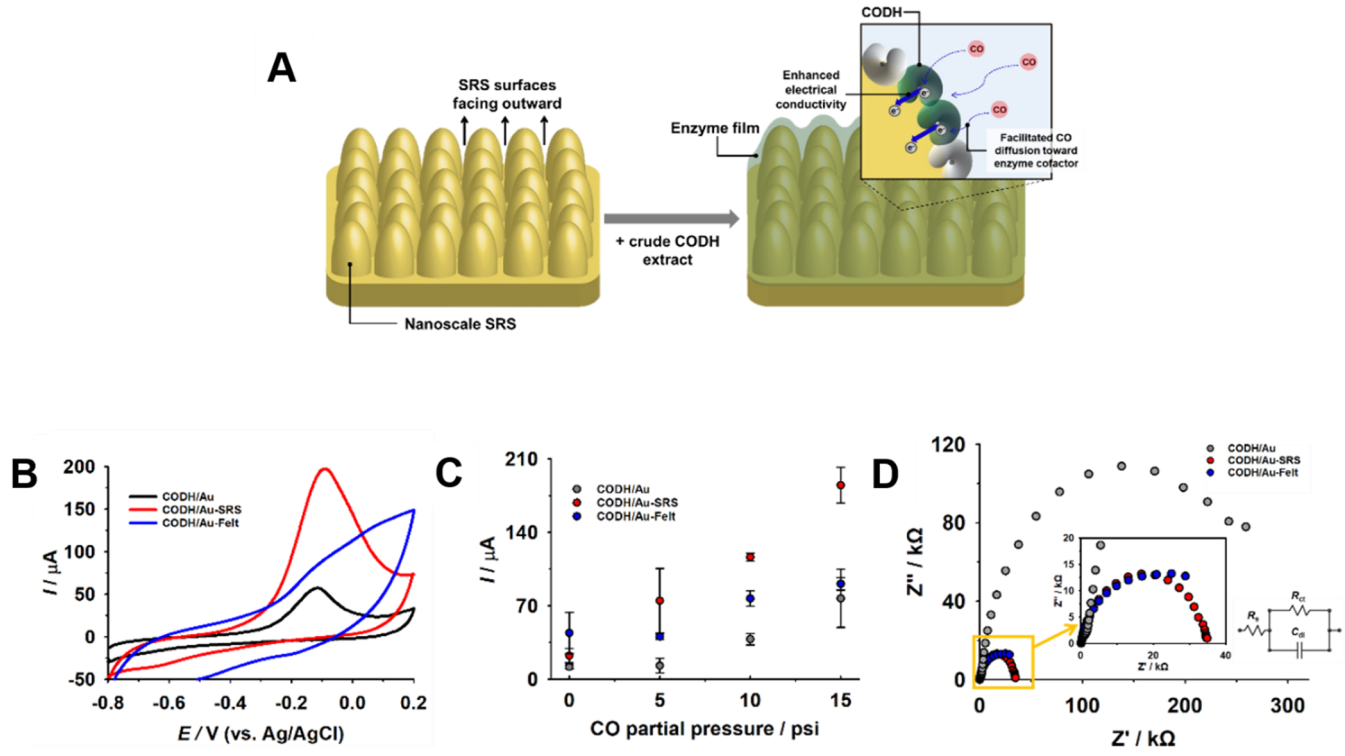

Fig. 3. (A) Schematic images describing the crude CODH on the Au-SRS (B) CV of crude CODH immobilized on Au-SRS, Au-felt, and plane Au electrode. (C) Plot of I_{peak} in the CV of crude CODH immobilized on Au, Au-SRS and Au-felt under various CO partial pressure (0–15 psi). (D) Nyquist plots of crude CODH immobilized on Au-SRS, Au-felt, and plane Au electrode.

enhanced as well, compared with those of CODH/Au. CODH/Au-SRS showed a steep increase in peak current at the quite negative potential of −100 mV (*vs.* Ag/AgCl). Meanwhile, Au-felt showed an extreme positive shift of peak potential and relatively low electrocatalytic current compared with those of CODH/Au-SRS (Fig. 3B).

The CV peak currents were then plotted against CO partial pressure for pressure values between 0 and 15 psi to estimate the electrochemical K_M^{app} values (Fig. 3C). The K_M^{app} values for CODH/Au, CODH/Au-SRS and CODH/Au-felt were in this way calculated to be 1.85, 1.12 and 2.22 mM, respectively. Here, the much lower K_M^{app} for CODH/Au-SRS than for CODH/Au implied that access of CO to the enzyme redox site was increased, i.e., the barrier to the diffusion of CO was decreased, as a result of modifying the electrode surface with the SRS. This result was assumed to be due to an increased distribution of enzyme molecules on the surface of the SRS, and hence an improved diffusion of CO toward the enzyme cofactors. On the other hand, the substrate-enzyme binding affinity for CODH/Au-felt was calculated to be ~20% less than that for CODH/Au, implying that the mass transfer of CO inside the micro-structured electrode was less favorable than the mass transfers in the nanoscale SRS as well as plane Au electrode.

In addition, the R_{ct} at the enzyme-electrode interface was estimated from the results of the EIS test to be 34.9 and 41.2 kΩ for CODH/Au-SRS and CODH/Au-felt, respectively (Fig. 3D). Both the Au-SRS and Au-felt electrodes were fabricated with the aim of achieving higher sensitivity by loading the enzymes on high surface area electrodes. However, the CODH/Au-felt showed an ~6.3 kΩ higher overpotential during ET at the enzyme-electrode interface than did CODH/Au-SRS although the same amount of enzyme was immobilized in each case.

All of the electrochemical parameters including K_M^{app}, I_{max}, and R_{ct} of the CODH-electrodes as well as dissolved CO concentration detection range are listed in Table 1, and were found to depend on the topography of the electrode surface. As shown in Table 1, the enzyme loadings on Au-SRS and Au-felt yielded enhancement of the DET kinetics. However, the interfacial ET of CODH on Au-felt was observed to

Table 1
Types of CODH-electrodes and electrochemical parameters.

Enzyme-electrode	K_M^{app} (mM)	I_{max} (μA)	R_{ct} (kΩ)	Detection range
CODH/Au	1.85	84.03	286.30	~190 (μM)
CODH/Au10	0.87	188.7	32.75	ND
CODH/Au40	1.51	166.7	58.85	ND
CODH/Au80	1.89	109.9	429.20	ND
CODH/Au-SRS	1.12	357.1	34.90	~488 (μM)
CODH/Au-felt	2.22	322.6	41.20	ND

ND: Not determine.

be sluggish compared with that of CODH/Au. This sluggishness was associated with its relatively high interfacial R_{ct} and reduced affinity for CO as indicated by its low K_{app}^{M}. This sluggishness indicated that the CODH/Au-felt solid support was not very effective at obtaining electrons produced by CO oxidation at the enzyme cofactor. It is assumed that the surface structure of Au-felt was extensive scale for film formation of nanometer-sized enzyme to be controlled, reducing the access of the cofactor to the electrode surface as well as precluding a uniform enzyme distribution, and hence significantly decreasing the electrical conductivity of enzyme cofactors with the electrode. Previously, it was also confirmed that R_{ct} increased with increasing particle size of the AuNP array, with the R_{ct} of Au80 (where the electrical penetration of the AuNPs was shown to be lower than those of other types of AuNP arrays) indicated to be one order magnitude higher than that of Au10 (Lee et al., 2018b). Also, the comparison of dissolved CO concentration detection range of CODH/Au and CODH/Au-SRS shows that linear range is only up to 190 μM for CODH/Au and 488 μM for CODH/Au-SRS. This could be attributed to the enhancement of DET at enzyme-electrode interface for CODH/Au-SRS.

The observed lower interfacial electrical conductivity of the more coarsely micro-structured enzyme-electrode suggested that the last electron donor in CODH, i.e., the [2Fe-2S] cluster, which is embedded in the ET subunits and known to be exposed to solvent, would be more

accessible on a finely tuned nanostructured electrode surface. These suggestions are applicable only for such enzymes that possess ET subunits with an electron-donating cofactor exposed to solvent. The DET capacity of an enzyme without an ET subunit is less likely to have an impact on micro- and nano-topographical electrodes, and in some cases may make the ET efficiency lower than that using an unmodified electrode. Thus, an enzyme harboring an ET subunit as well as a finely tuned nano-topographical electrode would appear to be prerequisites for efficient DET-based bioelectronics.

4. Conclusions

Here, immobilization of CODH on AuNP array with relatively small AuNPs yielded improved affinity for dissolved CO, which could be attributed to the enzymes having been distributed as a monolayer or near-monolayer, thereby increasing CO mass transfer toward enzyme. Furthermore, the nanoscale SRS endowed CODH cofactor with more electrical access to the electrode surface, resulted in less enzyme agglomeration and thus better substrate accessibility. Altogether, fine-tuning of the electrode surface structure on nanoscale greatly enhanced the electrical access of CODH cofactor to the electrode surface. This platform serves as an important step towards optimizing CODH biosensors for monitoring dissolved CO concentration.

CRediT authorship contribution statement

Stacy Simai Reginald: Investigation, Methodology, Validation, Writing - original draft, Writing - review & editing. **Hyeryeong Lee:** Investigation, Methodology, Validation, Writing - original draft, Visualization. **Yoo Seok Lee:** Conceptualization, Methodology. **Muhammad Yasin:** Writing - original draft. **In Seop Chang:** Supervision, Project administration, Funding acquisition.

Declaration of Competing Interest

The authors declare that they have no known competing financial interests or personal relationships that could have appeared to influence the work reported in this paper.

Acknowledgements

S.S. Reginald and H. Lee contributed equally. This work was supported by grants from the National Research Foundation of Korea (NRF), funded by the Korean Government (2016R1A2B3015426).

Appendix A. Supplementary data

Supplementary data to this article can be found online at https://doi.org/10.1016/j.biortech.2019.122436.

References

Barsan, M.M., Ghica, M.E., Brett, C.M., 2015. Electrochemical sensors and biosensors based on redox polymer/carbon nanotube modified electrodes: a review. Anal. Chim. Acta 881, 1–23.
Bradford, M.M., 1976. A rapid and sensitive method for the quantitation of microgram quantities of protein utilizing the principle of protein-dye binding. Anal. Biochem. 72, 248–254.
Chen, J., Zhu, R., Huang, J., Zhang, M., Liu, H., Sun, M., Wang, L., Song, Y., 2015. A glucose biosensor based on glucose oxidase immobilized on three-dimensional porous carbon electrodes. Analyst 140, 5578–5584.
Ding, S.-N., Holzinger, M., Mousty, C., Cosnier, S., 2010. Laccase electrodes based on the combination of single-walled carbon nanotubes and redox layered double hydroxides: towards the development of biocathode for biofuel cells. J. Power Sources 195, 4714–4717.
Dobbek, H., Gremer, L., Kiefersauer, R., Huber, R., Meyer, O., 2002. Catalysis at a dinuclear [CuSMo(=O)OH] cluster in a CO dehydrogenase resolved at 1.1-A resolution. Proc. Natl. Acad. Sci. U. S. A. 99 (25), 15971–15976.
Dobbek, H., Gremer, L., Meyer, O., Huber, R., 1999. Crystal structure and mechanism of CO dehydrogenase, a molybdo iron-sulfur flavoprotein containing S-selanylcysteine. Proc. Natl. Acad. Sci. U. S. A. 96 (16), 8884–8889.
Do, T., Varničić, M., Flassig, R., Vidaković-Koch, T., Sundmacher, K., 2015. Dynamic and steady state 1-D model of mediated electron transfer in a porous enzymatic electrode. Bioelectrochemistry 106, 3–13.
Freire, R.S., Pessoa, C.A., Mello, L.D., Kubota, L.T., 2003. Direct electron transfer: an approach for electrochemical biosensors with higher selectivity and sensitivity. J. Braz. Chem. Soc. 14, 230–243.
Goran, J.M., Mantilla, S.M., Stevenson, K.J., 2013. Influence of surface adsorption on the interfacial electron transfer of flavin adenine dinucleotide and glucose oxidase at carbon nanotube and nitrogen-doped carbon nanotube electrodes. Anal. Chem. 85, 1571–1581.
Houseman, B.T., Mrksich, M., 1999. The role of ligand density in the enzymatic glycosylation of carbohydrates presented on self- assembled monolayers of alkanethiolates on gold. Angew. Chem.-Int. Edit. 38, 782–785.
Ispas, C.R., Crivat, G., Andreescu, S., 2012. Review: recent developments in enzyme-based biosensors for biomedical analysis. Anal. Lett. 45 (2–3), 168–186.
Jang, N., Yasin, M., Park, S., Lovitt, R.W., Chang, I.S., 2017. Determination of volumetric gas-liquid mass transfer coefficient of carbon monoxide in a batch cultivation system using kinetic simulations. Bioresour Technol. 239, 387–393.
Jeong, Y., Jang, N., Yasin, M., Park, S., Chang, I.S., 2016. Intrinsic kinetic parameters of Thermococcus onnurineus NA1 strains and prediction of optimum carbon monoxide level for ideal bioreactor operation. Bioresour. Technol. 201, 74–79.
Kamin, R.A., Wilson, G.S., 1980. Rotating ring-disk enzyme electrode for biocatalysis kinetic studies and characterization of the immobilized enzyme layer. Anal. Chem. 52, 1198–1205.
Lee, H., Lee, Y.S., Lee, S.K., Baek, S., Choi, I.-G., Jang, J.-H., Chang, I.S., 2018a. Significant enhancement of direct electric communication across enzyme-electrode interface via nano-patterning of synthetic glucose dehydrogenase on spatially tunable gold nanoparticle (AuNP)-modified electrode. Biosens. Bioelectron. 126, 170–177.
Lee, S.W., Lee, K.Y., Song, Y.W., Choi, W.K., Chang, J., Yi, H., 2016. Direct electron transfer of enzymes in a biologically assembled conductive nanomesh enzyme platform. Adv. Mater. 28, 1577–1584.
Lee, Y.S., Baek, S., Lee, H., Reginald, S.S., Kim, Y., Kang, H., Choi, I.-G., Chang, I.S., 2018b. Construction of uniform monolayer-and orientation-tunable enzyme electrode by a synthetic glucose dehydrogenase without electron-transfer subunit via optimized site-specific gold-binding peptide capable of direct electron transfer. ACS Appl. Mater. Interfaces 10, 28615–28626.
Love, J.C., Estroff, L.A., Kriebel, J.K., Nuzzo, R.G., Whitesides, G.M., 2005. Self-assembled monolayers of thiolates on metals as a form of nanotechnology. Chem. Rev. 105, 1103–1170.
Maly, J., Krejci, J., Ilie, M., Jakubka, L., Masojidek, J., Pilloton, R., Sameh, K., Steffan, P., Stryhal, Z., Sugiura, M., 2005. Monolayers of photosystem II on gold electrodes with enhanced sensor response—effect of porosity and protein layer arrangement. Anal. Bioanal. Chem. 381, 1558–1567.
Marcus, R.A., Sutin, N., 1985. Electron transfers in chemistry and biology. Biochim. Biophys. Acta-Bioenerg. 811, 265–322.
Meyer, O., Gremer, L., Ferner, R., Ferner, M., Dobbek, H., Gnida, M., Meyer-Klaucke, W., Huber, R., 2000. The role of Se, Mo and Fe in the structure and function of carbon monoxide dehydrogenase. Biol. Chem. 381, 865–876.
Meyer, O., Schlegel, H.G., 1983. Biology of aerobic carbon monoxide-oxidizing bacteria. Annu. Rev. Control 37, 277–310.
Milton, R.D., Minteer, S.D., 2017. Direct enzymatic bioelectrocatalysis: differentiating between myth and reality. J. R. Soc. Interface 14 (131), 20170253.
Munasinghe, P.C., Khanal, S.K., 2014. Evaluation of hydrogen and carbon monoxide mass transfer and a correlation between the myoglobin-protein bioassay and gas chromatography method for carbon monoxide determination. RSC Adv. 4 (71), 37575–37581.
Mutlu, S., Mutlu, M., Pişkin, E., 1998. A kinetic approach to oxidase based enzyme electrodes: the effect of enzyme layer formation on the response time. Biochem. Eng. J. 1, 39–43.
Nylander, T., Mattisson, C., Razumas, V., Miezis, Y., Håkansson, B., 1996. A study of entrapped enzyme stability and substrate diffusion in a monoglyceride-based cubic liquid crystalline phase. Colloid Surf. A-Physicochem. Eng. 114, 311–320.
Ragsdale, S.W., Enzymology of the Wood–Ljungdahl pathway of acetogenesis, Ann. N.Y. Acad. Sci. 1125 (1) (2008) 129–136.
Reginald, S.S., Lee, Y.S., Lee, H., Jang, N., Chang, I.S., 2019. Electrocatalytic and biosensing properties of aerobic carbon monoxide dehydrogenase from Hydrogenophaga pseudoflava immobilized on Au electrode towards carbon monoxide oxidation. Electroanalysis 31 (9), 1635–1640.
Song, Y.M., Park, G.C., Kang, E.K., Yeo, C.I., Lee, Y.T., 2013. Antireflective grassy surface on glass substrates with self-masked dry etching. Nanoscale Res. Lett. 8, 505.
Varničić, M., Bettenbrock, K., Hermsdorf, D., Vidaković-Koch, T., Sundmacher, K., 2014. Combined electrochemical and microscopic study of porous enzymatic electrodes with direct electron transfer mechanism. RSC Adv. 4, 36471–36479.
Yasin, M., Jeong, Y., Park, S., Jeong, J., Lee, E.Y., Lovitt, R.W., Kim, B.H., Lee, J., Chang, I.S., 2015. Microbial synthesis gas utilization and ways to resolve kinetic and mass-transfer limitations. Bioresour. Technol. 177, 361–374.
Ye, X., Huang, J., Geng, F., Sun, L., Liu, H., Jiang, X., Wu, W., Zu, X., Zheng, W., 2016. broadband antireflection subwavelength structures on fused silica using lower temperatures normal atmosphere thermal dewetted Au nanopatterns. IEEE Photonics J. 8, 1–10.
Zebda, A., Gondran, C., Le Goff, A., Holzinger, M., Cinquin, P., Cosnier, S., 2011. Mediatorless high-power glucose biofuel cells based on compressed carbon nanotube-enzyme electrodes. Nat. Commun. 2, 370.
Zhang, C., Luo, S., Chen, W., 2013. Activity of catalase adsorbed to carbon nanotubes: effects of carbon nanotube surface properties. Talanta 113, 142–147.